Plxdc family members are novel receptors for the rhesus monkey rhadinovirus (RRV)

Anna K. Großkopf[1], Sarah Schlagowski[1], Armin Ensser[2], Ronald C. Desrosiers[3], Alexander S. Hahn[1]

[1] German Primate Center - Leibniz Institute for Primate Research, Göttingen, Germany

[2] Universitätsklinikum Erlangen, Institute for Clinical and Molecular Virology, Erlangen, Germany

[3] Miller School of Medicine, University of Miami, Miami, United States

ABSTRACT

The rhesus monkey rhadinovirus (RRV), a γ2-herpesvirus of rhesus macaques, shares many biological features with the human pathogenic Kaposi's sarcoma-associated herpesvirus (KSHV). Both viruses, as well as the more distantly related Epstein-Barr virus, engage cellular receptors from the Eph family of receptor tyrosine kinases (Ephs). However, the importance of the Eph interaction for RRV entry varies between cell types suggesting the existence of Eph-independent entry pathways. We therefore aimed to identify additional cellular receptors for RRV by affinity enrichment and mass spectrometry. We identified an additional receptor family, the Plexin domain containing proteins 1 and 2 (Plxdc1/2) that bind the RRV gH/gL glycoprotein complex. *In vitro,* blocking assays with soluble Plxdc2 decoy receptor reduced RRV infection by approx. 60%, while overexpression of Plxdc1 and 2 dramatically enhanced RRV susceptibility in otherwise marginally permissive Raji cells. While the Plxdc2 interaction is conserved between two RRV strains, 26-95 and 17577, Plxdc1 specifically interacts with RRV 26-95 gH. The Plxdc interaction is mediated by a short motif at the N-terminus of RRV gH that is partially conserved between isolate 26-95 and isolate 17577, but absent in KSHV gH. Mutation of this motif abrogated the interaction with Plxdc1/2 in *in vitro* assays and reduced RRV infection in a cell-type specific manner. Taken together, our findings characterize Plxdc1/2 as novel interaction partners and entry receptors for RRV and support the concept of the N-terminal domain of the gammaherpesviral gH/gL complex as a multifunctional receptor-binding domain.

INTRODUCTION

The rhesus monkey rhadinovirus (RRV), a member of the genus γ2-herpesvirus or rhadinovirus, is closely related to the only human pathogenic member of this genus, the Kaposi's sarcoma associated herpesvirus (KSHV) (1, 2). Due to the high similarity in both genome organization and biology RRV is considered as an animal model virus for KSHV (3) and has been used as such in various *in vitro* and *in*

33 *vivo* studies. Two major RRV sequence groups have been identified (4), which are represented by two
34 cloned isolates, RRV 26-95 (5) and RRV 17577 (6). Analogous to KSHV infection, primary RRV infection
35 is asymptomatic in healthy hosts and leads to life-long persistence, most likely in the B cell
36 compartment (7). KSHV is associated with a solid tumor of endothelial origin, Kaposi's sarcoma (KS),
37 and two B cell malignancies, primary effusion lymphoma (PEL) and the plasmablastic variant of
38 multicentric Castleman's disease (MCD), most prominently in the context of human
39 immunodeficiency virus (HIV) infection and in immunocompromised individuals. Similarly, simian
40 immunodeficiency virus (SIV)-positive rhesus macaques developed B cell lymphomas upon
41 experimental infection with RRV strain 17577 (8, 9) and several studies correlated RRV infection with
42 lymphomagenesis in SIV/SHIV-infected animals (10, 11). While RRV is not consistently associated
43 with solid malignancies, RRV has been identified in retroperitoneal fibromatosis tissue (9, 12), similar
44 to retroperitoneal fibromatosis herpesvirus (RFHV)(11). Another shared characteristic of KSHV and
45 RRV is the receptor usage on a range of cell types. Both viruses engage members of the Eph family of
46 receptor tyrosine kinases (Ephs) through their glycoprotein (g)H/gL complex to facilitate entry into
47 target cells. While KSHV preferentially interacts with A-type Ephs – specifically EphA2 as the high
48 affinity receptor (13, 14) – RRV can utilize both A- and B-type Ephs (14) for entry. These interactions
49 have been characterized on different adherent cells types (6–9) and we could recently show that
50 both viruses can utilize EphA7 as receptor on BJAB cells (19), a model B lymphocyte line. While for
51 KSHV, in addition to Eph family receptors, several membrane proteins have been proposed as cellular
52 receptors for different viral glycoproteins mediating either attachment or entry on a range of target
53 cells (reviewed in (20)) the receptor usage of RRV is comparatively less well characterized.
54 Nevertheless, studies using receptor knock-down, receptor- and ligand-mediated blocking, and Eph
55 de-targeted virus mutants (21) showed that both viruses can infect various cells independently of the
56 Eph-interaction, which suggests that RRV engages at least one additional entry receptor that can
57 functionally substitute for the Eph-interaction. This notion is also supported by a recent *in vivo* study
58 that demonstrated that an RRV mutant deleted of gL and therefore unable to interact with Eph
59 receptors still establishes persistent infection in RRV-naïve rhesus macaques upon intravenous
60 inoculation (22). We therefore aimed to identify additional rhadinovirus receptors that bind the
61 gH/gL complex or gH and identified Plexin domain containing protein 2 (Plxdc2) as novel interaction
62 partner of the gH/gL complex of RRV, but not KSHV. The closest homolog to Plxdc2, Plxdc1 was
63 initially identified as overexpressed in blood vessels of solid human tumors (23), resulting in the
64 original terminology tumor endothelial marker 7 (TEM7, Plxdc1) and tumor endothelial marker 7
65 related (TEM7R, Plxdc2) (24). In general, the physiological functions of Plxdc1/2 are not well
66 understood. Suggestive of a role in development, Plxdc2 has been described as mitogen for neural
67 progenitor cells (25) and expression of both Plxdc1 and Plxdc2 in the developing nervous system has

68 been demonstrated (26, 27). Cortactin, nidogen and the pigment epithelium derived factor (PEDF)
69 have been described as interactors for Plxdc1 and Plxdc2 (28–30). However, the physiological
70 relevance of these interactions is not fully understood. In this study we characterize the interaction
71 of Plxdc1/2 with the gH/gL glycoprotein complex of RRV and establish Plxdcs as novel cellular RRV
72 entry receptors.

73

74 **RESULTS**

75 To identify potential cellular receptors for RRV glycoprotein H, we performed
76 immunoprecipitation using soluble RRV 26-95 gH, consisting of the extracellular part fused to the Fc
77 part of human IgG (RRV gH-FcStrep) as bait and 293T whole cell lysate as prey (Fig 1A). Bands present
78 in the precipitation from 293T whole cell lysate, but not in control precipitation without 293T lysate
79 were excised and analyzed by LC-MS/MS. The most abundant cell surface protein, identified in four
80 of the five analyzed regions, was Plxdc2 or TEM7R, a cellular transmembrane protein. As described
81 above, Plxdc1 or TEM7 is the only homolog of Plxdc2 in humans and rhesus macaques, and was
82 therefore included in subsequent analyses. Human and rhesus Plxdc1 (ref |NM_020405.5|; ref
83 |XM_028836436.1|) and Plxdc2 (ref |NM_032812.9|; ref |XM_028826043.1|) are 96.80% and
84 97.92% identical on the amino sequence level.

85 Co-immunoprecipitation of V5-tagged expression constructs of gH from KSHV and from the
86 two RRV isolates 26-95 and 17577, in the presence or absence of the corresponding Flag-tagged gL
87 proteins with myc-tagged human Plxdc1 or Plxdc2 (hPlxdc1-myc/ hPlxdc2-myc) from transfected
88 293T cells confirmed the interaction of both RRV gH/gL complexes with Plxdc2 (Fig 1B). Neither KSHV
89 gH/gL nor RRV 17577 gH/gL interacted detectably with Plxdc1-myc, while RRV 26-95 prominently
90 bound both Plxdc1 and Plxdc2 in the presence and absence of gL.

91 To evaluate the effect of Plxdc-binding to RRV gH on the interaction with EphB3, the high-
92 affinity Eph family receptor for RRV gH/gL (14), we used soluble human Plxdc1 or Plxdc2, consisting
93 of the extracellular part of Plxdc1 or Plxdc2 fused to the Fc part of human IgG followed by a
94 TwinStrep tag (hPlxdc1-FcStrep/ hPlxdc2-FcStrep) in immunoprecipitation experiments. Co-
95 immunoprecipitation of hPlxdc1-FcStrep/ hPlxdc2-FcStrep with the gH-V5/gL-Flag complexes of RRV
96 isolates 26-95 and 17577 in the presence or absence of myc-tagged EphB3 from transfected 293T
97 cells demonstrated the existence of a quaternary complex, indicating the ability of RRV gH/gL to
98 interact with members of both receptor families simultaneously (Fig 1C).

99 While interaction in transfected cell lysates is strongly suggestive of a functional interaction,
100 the biologically relevant interaction for the entry process would occur with virion gH/gL. To evaluate

101 the functionality of the gH/gL – Plxdc interaction on virus particles both for wildtype RRV and an Eph-
102 binding-negative RRV mutant, we utilized RRV-YFP, an RRV 26-95 strain engineered for constitutive
103 YFP expression upon infection, and RRV-YFP gH-AELAAN, an Eph-binding-negative RRV-YFP mutant
104 that we had previously described (Fig 2A) (21). To analyze the impact of competition with soluble
105 Plxdc decoy receptor, RRV-YFP and RRV-YFP gH-AELAAN preparations were incubated with a
106 concentration series of soluble hPlxdc2-FcStrep or an FcStrep control prior to infection of HaCaT cells
107 (Fig 2B). According to RNA-Seq data of 36 cell lines (Courtesy of Human Protein Atlas,
108 www.proteinatlas.org, (31)), HaCaT cells exhibit the highest cell-line specific expression of Plxdc2
109 among the analyzed non-cancer cell lines and were therefore chosen for further analyses. Soluble
110 Plxdc2-FcStrep inhibited RRV-YFP wt infection up to approx. 60% in a dose dependent manner when
111 compared to FcStrep alone. Likewise, preincubation of RRV-YFP gH-AELAAN with hPlxdc2-FcStrep
112 reduced infection by approx. 65%. RRV wt and RRV gH-AELAAN infection was normalized to approx.
113 MOI 0.2. Inhibition of the gH/gL-Eph interaction, which served as control, lead to an approx. 50%
114 reduction of RRV wt infection at a concentration of 10nM hEphB3-Fc while 100nM of soluble
115 hPlxdc2-FcStrep exhibited a similar blocking efficiency. Preincubation with both hEphB3-Fc and
116 hPlxdc2-FcStrep further reduced RRV wt infection on HaCaT cells, when compared to preincubation
117 with either hEphB3-Fc or hPlxdc2-FcStrep alone (Fig 2C). While preincubation with EphB3-Fc did not
118 reduce RRV gH-AELAAN infection, preincubation with either hPlxdc2-FcStrep or a combination of
119 hPlxdc2-FcStrep and hEphB3-Fc reduced infection by approx. 50% as observed for RRV wt infection
120 (Fig 2C). Infection of SLK cells and rhesus monkey fibroblasts was also slightly decreased by
121 preincubation of the viral inoculum with hPlxdc2-FcStrep, infection of SLK by RRV-YFP wt to 63.5% ±
122 3.7% and infection of RF by RRV-YFP wt to 73.9% ± 11.3% relative to preincubation with FcStrep as
123 control. However, this effect was less pronounced than on HaCaT and less pronounced than the
124 effect of hPlxdc2-FcStrep on RRV gH-AELAAN infection of the same cell types (Fig 2D). Taken
125 together, the immunoprecipitation and blocking experiments confirm the independence of the
126 gH-Plxdc interaction of the previously described Eph-interaction motif (21) and EphB3-binding.

127 To establish receptor function, we performed gain-of-function experiments using ectopic
128 Plxdc1/2 overexpression. Raji cells were transduced with lentiviruses encoding TwinStrep-tagged
129 human Plxdc1/2 constructs (hPlxdc1-Strep/ hPlxdc2-Strep). The EBV-positive, human lymphoblast
130 cell line only allows for low-level RRV 26-95 infection even with amounts of input virus corresponding
131 to high MOI on adherent cells like SLK, HaCaT or RF. Therefore, changes in susceptibility to infection,
132 mediated by Plxdc1/2 overexpression should be readily detectable and allow for a clear
133 differentiation of the contribution of Plxdc1/2 to RRV infection over the very low intrinsic
134 susceptibility to infection. Indeed, ectopic expression of hPlxdc1/2-Strep increased RRV-YFP wt and
135 RRV-YFP gH-AELAAN infection 40 to 60-fold from approx. 0.5% basal infection dependent on the

136 expression plasmid and RRV strain (Fig 2E, G). However, we did not observe pronounced differences
137 in effects mediated by hPlxdc1-Strep or hPlxdc2-Strep, indicating no clear Plxdc receptor preference
138 of RRV 26-95.

139 In a next step we characterized the Plxdc binding motif on RRV gH. As the RRV 17577 gH-
140 Plxdc2 interaction depends on gL whereas the RRV 26-95 gH-Plxdc2 interaction does not, we focused
141 on the N-terminal domain I of gH which, in analogy to EBV gH/gL (32), most likely constitutes the gL-
142 binding interface. The differences in the Plxdc interaction of RRV isolates 26-95 and 17577 as well as
143 the lack of Plxdc – KSHV gH/gL interaction suggested a motif that is only partially conserved between
144 the RRV isolates but missing in KSHV. Using sequence comparisons (Fig 3A) we identified a putative
145 interaction motif spanning 7 or 6 amino acid motif in the N-terminal region of RRV 26-95 gH and RRV
146 17577 gH, respectively, that is not conserved in KSHV gH. The motif is located close to the Eph-
147 interaction motif we described previously, facing in the opposite direction in a homology model of
148 the RRV 26-95 gH/gL complex based on the EBV gH/gL crystal structure (3PHF) (Fig 3B). Deletion of
149 this motif completely abrogated the gH/gL interaction with Plxdcs of both RRV 26-95 (Fig 3C) and RRV
150 17577 (Fig 3D). To further characterize the contribution of individual residues in the 'Tyr(Y)-Glu(E)-
151 Tyr(Y)-Asn(N)-Glu(E)-Glu(E)-Lys(K)' (RRV 26-95) motif we performed single amino acid substitutions
152 to alanine. The ability of mutant RRV 26-95 gH-V5 to bind myc-tagged Plxdc1/2 of human (hPlxdc1/2-
153 myc) (Fig 3E) or rhesus macaque origin (mmPlxdc1/2-myc) (Fig 3F) was analyzed by
154 immunoprecipitation of gH via the V5-tag and Western blot. While several single amino acid
155 substitutions decreased the interaction of RRV gH with Plxdcs to some degree, residues Tyr23 and
156 Glu25 that are conserved in isolates 26-95 and 17577 appear to be critical for the interaction of gH
157 with human and rhesus macaque Plxdc1 and Plxdc2. Furthermore, substitution of glutamate with
158 alanine at position 22, which is not conserved between isolates 26-95 and 17577, had a pronounced,
159 albeit slightly weaker effect on the gH-Plxdc1/2 interaction (Fig 3E, F).

160 To further analyze the contribution of the gH/gL – Plxdc interaction in the context of infection
161 we constructed virus mutants deleted in the seven amino acid interaction motif in the background of
162 RRV-YFP 26-95 wildtype (RRV gHΔ21-27), and in the background of an RRV-YFP 26-95 strain mutated
163 in the Eph-interaction motif described previously by our group (RRV gH-AELAAN, RRV gHΔ21-27-
164 AELAAN) using a two-step, lambda red-mediated recombination system (33) (Fig 4A). Blocking
165 experiments using soluble hPlxdc2-FcStrep decoy receptor on HaCaT cells confirmed that deletion of
166 the seven amino acid motif was sufficient to abrogate the gH-Plxdc2 interaction on viral particles (Fig
167 4B). While infection of RRV wt and RRV gH-AELAAN was inhibited by approx. 60% to 70%
168 respectively, infection of RRV gHΔ21-27 and RRV gHΔ21-27-AELAAN was not affected even by high
169 concentrations of soluble hPlxdc2-FcStrep (Fig 4B). All infections were carried out at approx. MOI

170 0.05. Analogously, the Eph- or Plxdc-receptor-binding-negative RRV mutants were no longer inhibited
171 by preincubation with the respective soluble receptor (hEphB3-Fc or hPlxdc2-FcStrep) in single or
172 double inhibition experiments on HaCaT cells (Fig 4C). The receptor-specificity conveyed by the
173 respective interaction motif was further analyzed in lentiviral vector-mediated Plxdc1/2-Strep
174 overexpression experiments in Raji B lymphocytes. EphA7, which had previously been described by
175 our group to be critical for RRV infection of BJAB B lymphocytes, was used as control for Eph-
176 mediated infection. Expression of Plxdc1/2-Strep as well as EphA7-Strep dramatically enhanced
177 susceptibility of Raji cells (Fig 4D, E). RRV-YFP wt infection increased from 0.14 ± 0.04% on empty
178 vector transduced Raji cells to approx. 8.5% upon EphA7 overexpression and to approx. 17% upon
179 Plxdc1/2 overexpression, without pronounced differences between the Plxdc family members.
180 Mutation of the Eph-interaction motif in RRV-YFP gH-AELAAN completely abrogated the gain in
181 susceptibility on EphA7 overexpressing cells while mutation of the Plxdc-interaction motif completely
182 abrogated the gain in susceptibility on Plxdc1/2 overexpressing cells, confirming selective knockout
183 of each individual receptor interaction in the respective mutant. Furthermore, deletion of the Eph-
184 interaction motif in RRV-YFP gH-AELAAN did not impact the infection of Plxdc1/2 overexpressing cells
185 in comparison to RRV-YFP wt infection. In contrast, we observed an approx. 2-fold higher infection of
186 RRV-YFP gHΔ21-27 on EphA7 overexpression cells, when compared to RRV-YFP wt. Together, the
187 blocking and overexpression experiments indicate an independent rather than cooperative nature of
188 Eph and Plxdc receptor function.

189 To quantitatively analyze the contribution of the Plxdc1/2-interaction to RRV infection of
190 different cell types, RRV-YFP wt and RRV-YFP receptor binding mutant inocula were normalized to
191 genome copies as determined by qPCR, and target cells were inoculated with the same number of
192 encapsidated input virus genomes for wt and each mutant virus strain in an MOI range of 0.05 to 1
193 on adherent cells. Infection as determined by the percentage of YFP+ cells was normalized to RRV wt,
194 which was set to 1. For suspension cell lines, experiments with RRV wt infection over 1% were
195 included in the analysis. Four (three for RF, five for MFB5487) independent sets of RRV wt and
196 mutant stocks were used to compensate for variability in stock preparation. None of the analyzed
197 adherent cell lines showed a preferential use of Plxdc receptors over Eph receptors based on the
198 reduction of specific infectivity of Eph-binding and Plxdc-interaction-deficient mutants (Fig 5A). On
199 rhesus monkey fibroblasts (RF), compared to RRV-YFP, RRV-YFP gHΔ21-27, RRV-YFP gH-AELAAN and
200 RRV-YFP gHΔ21-27-AELAAN exhibited a decrease in infection of approx. 30%, 50% and 70%,
201 respectively. Similarly on HaCaT, infection with RRV-YFP gH-AELAAN and RRV-YFP gHΔ21-27-AELAAN
202 was reduced by approx. 60% and 75%, respectively, compared to RRV-YFP. While RRV-YFP gHΔ21-27
203 exhibited a defect, comparable to RRV-YFP gH-AELAAN in three of the analyzed independent sets of
204 RRV stocks, this reduction in infectivity did not reach significance due to one outlier. On SLK cells,

205 mutation of the Eph-interaction motif led to an approx. 65% decrease in infection, while RRV-YFP
206 gHΔ21-27 infection was on average comparable to RRV-YFP infection. In contrast, we identified B
207 lymphocyte lines of human and macaque origin that exhibit a preference in the receptor usage for
208 either Eph or Plxdc family members (Fig 5B). When normalized to genome copies, RRV-YFP gHΔ21-27
209 infection on human Raji lymphoblasts was comparable to RRV wt infection while mutation of the
210 Eph-interaction motif lead to an approx. 90% decrease in infection, indicating preferential infection
211 through Eph family receptors. Similarly, RRV-YFP gHΔ21-27 exhibited only a minor defect (approx.
212 20% reduced infection) on immortalized B lymphocytes of macaca mulatta origin (MMB1845) that
213 did not reach significance, while infection with RRV-YFP gH-AELAAN and gHΔ21-27-AELAAN was
214 reduced by approx. 90% in comparison to RRV-YFP, again indicating preferential infection through
215 Eph family receptors. Conversely, deletion of the Plxdc-interaction motif decreased infection of a B
216 lymphocyte cell line of macaca fascicularis origin (MFB5487) by approx. 75% whereas RRV-YFP gH-
217 AELAAN exhibited an approx. 50% defect, indicating preferential use of the Plxdc interaction for
218 infection of MFB5487 by RRV. Mutation of both the Eph- and Plxdc-interaction motif led to an even
219 more pronounced defect of approx. 90%.

220 To evaluate the contribution of potential attachment effects on the observed differences in
221 specific infectivity, we analyzed the capacity of virions to bind Plxdc1/2 overexpressing Raji cells in
222 comparison to empty vector transduced Raji cells (Fig 5C, D). The ratio of cell-bound viral DNA to
223 input genomes was used as a surrogate marker for virus attachment. Mutation of the Plxdc- and Eph-
224 interaction motif had no detectable effect on attachment to control vector-transduced and Plxdc2-
225 overexpressing Raji cells. In contrast, Raji cells overexpressing Plxdc1 showed increased attachment
226 of RRV-YFP 26-95 and RRV-YFP 26-95 gH-AELAAN, while attachment of Plxdc-interaction negative
227 RRV-YFP 26-95 mutants gHΔ21-27 and gHΔ21-27-AELAAN was not enhanced and remained
228 comparable to empty vector control and Plxdc2-overexpressing cells.

229 To exclude effects of potential offsite genomic rearrangements in RRV-YFP 26-95 gHΔ21-27
230 we created two independent revertants (RRV 26-95 gHΔ21-27^{rev9-4} and RRV 26-95 gHΔ21-27$^{rev10-3}$).
231 Restoration of the residues deleted in RRV-YFP 26-95 gHΔ21-27 restored infection on hPlxdc1/2-
232 transduced Raji, MFB5487 and HaCaT cells to RRV wt levels, with no pronounced differences
233 between RRV wt, RRV 26-95 gHΔ21-27^{rev9-4} and RRV 26-95 gHΔ21-27$^{rev10-3}$ (Fig 5E). Similar to the
234 approx. 11-fold increase of RRV wt infection upon hPlxdc1/2 overexpression, infection with RRV
235 gHΔ21-27 revertants increased from 2.00 ± 0.30% (2.54 ± 0.29%) on empty vector transduced Raji
236 cells to 35.25 ± 1.21% (36.99 ± 0.39%) and 37.27 ± 0.68% (43.00 ± 0.99%) upon hPlxdc1 and hPlxdc2
237 overexpression for RRV 26-95 gHΔ21-27^{rev9-4} (RRV 26-95 gHΔ21-27$^{rev10-3}$) respectively (Fig 5E).

238

239 **DISCUSSION**

240 In this study we identified the Plexin domain containing proteins 1 and 2 as a novel family of
241 entry receptors for RRV. Plxdc1/2 interact with the gH/gL complex of RRV in a region close to the
242 previously characterized binding motif for Eph receptors. While the Eph-interaction as well as the
243 critical Eph binding motif in domain I of gH is conserved between RRV and the closely related human
244 pathogenic KSHV (21), the interaction with Plxdc1/2 is exclusive to RRV and even exhibits differences
245 between isolates 26-95 and 17577 as prototypic members of the described RRV sequence clades.

246 According to our results, differences between Plxdc1 and Plxdc2 may also exist in terms of
247 function. While overexpression of both Plxdc1 and Plxdc2 in Raji cells, that were virtually "non-
248 susceptible" under the conditions used, lead to robust RRV 26-95 infection (Fig 4D-E), only
249 overexpression of Plxdc1 enhanced attachment of RRV wt and RRV gH-AELAAN in comparison to
250 either non-transduced Raji cells or Plxdc-binding deficient RRV mutants (Fig 5D). Whether this is
251 primarily due to differences in expression levels, consistently observed between Plxdc1 and Plxdc2
252 upon lentiviral overexpression or due to underlying functional differences in the gH interaction with
253 these molecules remains to be determined.

254 Mutation of residues Tyr23 and Glu25 in gH domain I which are conserved between RRV
255 isolate 26-95 and 17577 almost abolished the interaction with Plxdc2, which is bound by gH/gL of
256 both isolates. Although the same residues are critical for the interaction of RRV gH 26-95 with Plxdc1,
257 the partial conservation of the region appears to be insufficient to confer binding of 17577 gH to
258 Plxdc1. Interestingly, the interaction of 17577 gH with Plxdc2 is dependent on the presence of gL in
259 the gH/gL complex, whereas 26-95 gH is able to bind Plxdc1/2 independent of gL. These features of
260 Plxdc1/2 binding specificities appear similar to the interaction of the gH/gL complex with Eph
261 receptors, wherein mutation of the strictly conserved Eph interaction motif is sufficient to abrogate
262 receptor binding, but differences in KSHV and RRV affinities for A- and B-type Eph RTKs indicate the
263 existence of additional regions in gH or gL that contribute to or modulate the interaction. Whether
264 these preferences for different members of conserved receptor families also influence e.g. cell or
265 tissue tropism, viral spread or pathogenicity has not been determined. Sequence comparisons of
266 over twenty RRV isolates identified dramatic differences in the extracellular domains of gH as well as
267 in gL between isolates that fell in two discrete groupings either similar to 26-95 or 17577, while
268 variation in other glycoproteins R1, gM, gN, orf68 was minimal between clades (4). However, if these
269 clade-specific glycoprotein variations influence the observed differences in pathogenicity between
270 RRV strains 26-95 and 17577 remains to be seen. Another interesting question would be if the
271 receptor-binding function of the N-terminal region of gH is conserved between RRV and KSHV, and
272 probably EBV, and whether KSHV and EBV can bind another receptor through this region. So far, we

273 did not to identify corresponding interactions for KSHV, but in principle the region of gH is present in
274 both viruses and it is tempting to assume some functional conservation.

275 Along those lines, the evolutionary factors that drive interaction with different receptor
276 families and the resulting multitude of herpesvirus–receptor interactions is highly interesting. For e.g.
277 EBV and HCMV, a clear correlation between receptor usage, dependent on viral interaction partners
278 of the gH/gL complex, and cell tropism has been demonstrated in various studies ((34), reviewed in
279 (35)). However, for rhadinoviruses, the picture is less clear. Even though we could show that RRV
280 infection of select cell lines exhibited a dependence on specific receptors, e.g. Raji infection was
281 dependent on the gH/gL – Eph interaction, MFB5487 infection was more dependent on the Plxdc-
282 interaction (Fig 5) and similarly mutation of the Eph-interaction motif did not impact infection on all
283 cell types equivalently (21), a definite correlation between exclusive receptor usage and infection of
284 specific cell types is still missing. While the notion of a role of different receptor interactions in KSHV
285 and RRV cell and tissue tropism is tempting, the possibility of a redundant function should not be
286 discarded. Redundancy could be driven by the need to escape antibodies e.g. to one receptor binding
287 site. For instance, *in vitro* infection of human keratinocytes or rhesus fibroblasts seemed to be
288 impacted to a similar degree by either deletion of the Eph- or of the Plxdc-interaction motif (Fig 5).
289 To ultimately address the correlation between receptor- and tissue-tropism, *in vivo* studies using
290 receptor-de-targeted mutants to analyze cell and tissue tropisms will be required. The importance of
291 *in vivo* studies is also supported by a recent report that showed that a gL-null RRV mutant still
292 established persistent infection in the B cell compartment upon intravenous inoculation, while
293 infection of B cells *in vitro* was drastically reduced (22), a finding that could be explained by the gL-
294 independent usage of Plxdc1/2 for B cell infection *in vivo.*

295 On a more speculative note, the apparent overlap between virus receptors and tumor-
296 associated membrane proteins may represent an interesting research subject. Eph receptors were
297 first identified in an attempt to characterize tyrosine kinases involved in cancer (36) and altered
298 expression in various cancer types has been demonstrated for several Eph family members (reviewed
299 in (37)). Similarly, Plxdc1 was first described in a screen for novel tumor endothelial members (23)
300 and expression of both Plxdc1 and Plxdc2 is elevated in the endothelium of solid tumors (23, 24, 38,
301 39). Plxdc1 expression has been described as prognostic marker and modulating factor for various
302 human cancers (38–42). Given the similarity in changes of e.g. metabolic, transcriptional, and
303 signaling networks in cancer cells and upon virus infection it is not unlikely that either elevated
304 expression or signaling of these molecules is favorable for both virus infection and cancer
305 progression.
306
307

308 **FIGURES**

309

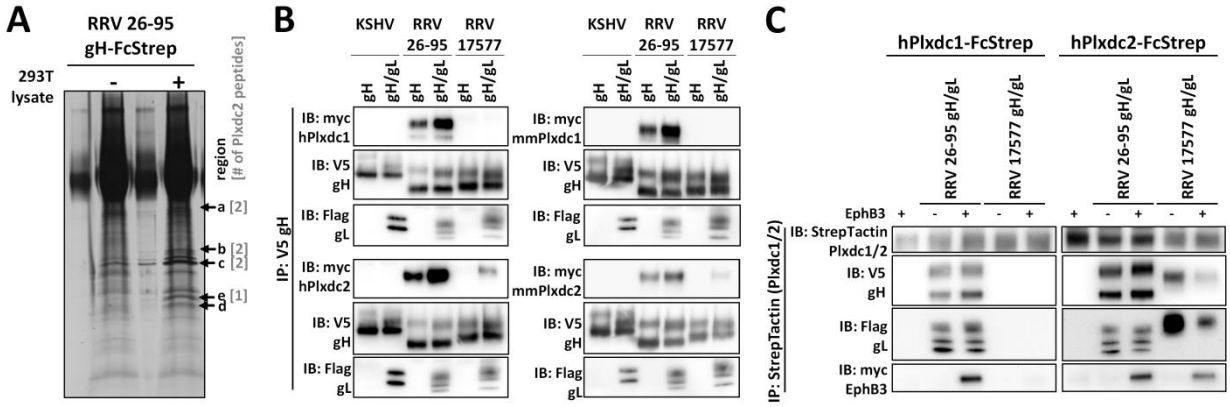

310

311 **Figure 1 Plxdc family receptors are novel interaction partners for the RRV gH/gL**. **A)**
312 Immunoprecipitation of recombinant soluble RRV 26-95 gH-FcStrep in the presence or absence of
313 293T lysate. Precipitates were analyzed by PAGE, silver stained and bands at the indicated molecular
314 weight (arrows, regions a-d) were excised and analyzed by mass spectrometry. Numbers in brackets
315 indicate the number of Plxdc2 peptides identified by LC-MS/MS in each region. **B)** V5-tagged RRV
316 26-95 gH, RRV 17577 gH or KSHV gH alone or co-expressed with the respective Flag-tagged gL
317 construct were immunoprecipitated in the presence of full-length Plxdc1 or Plxdc2 from human (h) or
318 macaca mulatta (mm) origin using monoclonal antibody to the V5-tag. Precipitates were analyzed by
319 Western blot with the indicated antibodies. **C)** Co-immunoprecipitation of soluble human Plxdc1-
320 FcStrep or human Plxdc2-FcStrep with RRV 26-95 gH-V5/gL-Flag or RRV 17577 gH-V5/gL-Flag using
321 StrepTactin Sepharose in the presence or absence of human full-length EphB3. Abbreviations: IP:
322 immunoprecipitation, IB: immunoblotting, h: human, mm: macaca mulatta (rhesus macaque).

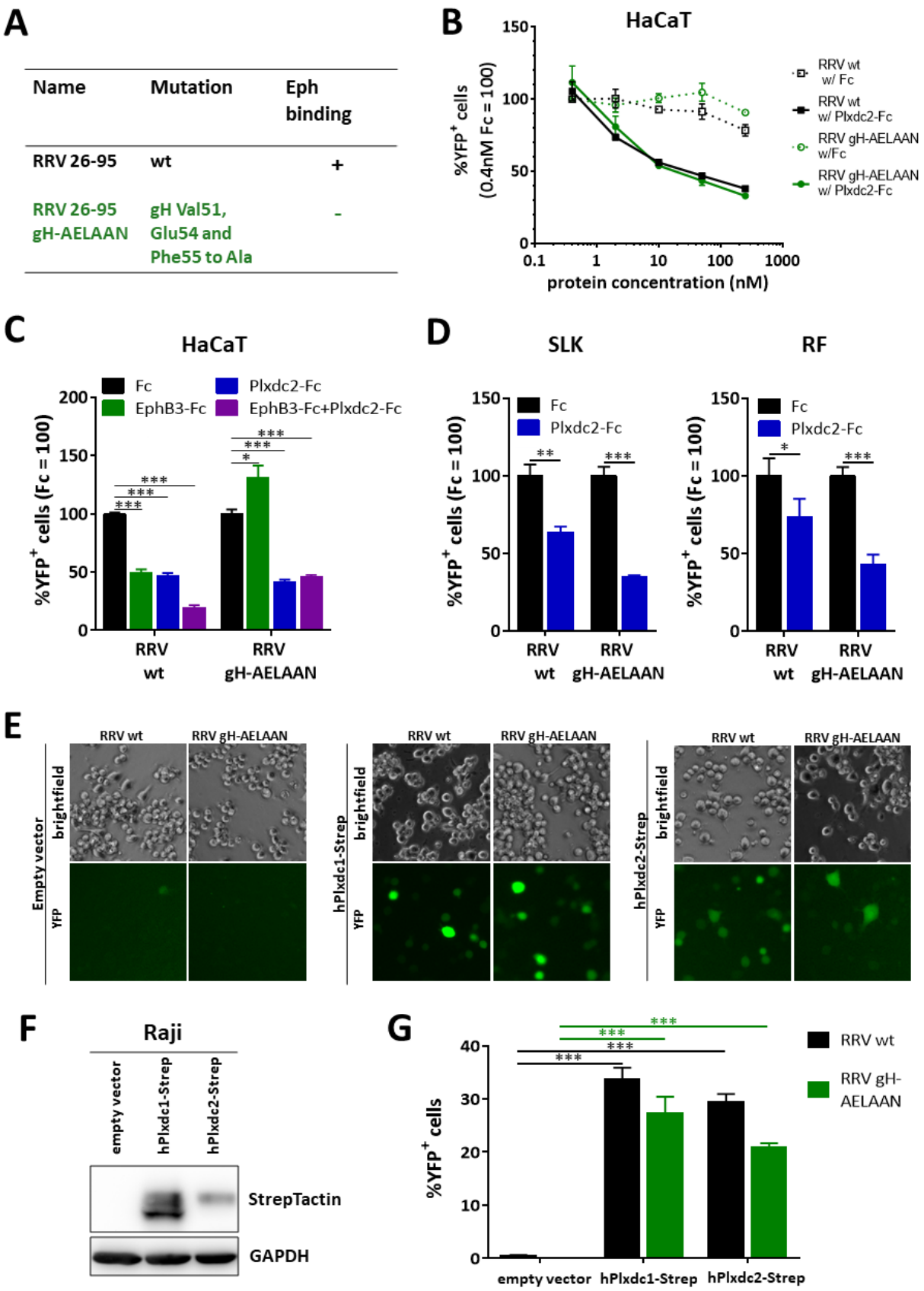

Figure 2 Plxdc1/2 function as entry receptors for RRV. A) List of BAC-derived recombinant viruses and introduced mutations used in this figure. **B)** Dose-dependent inhibition of RRV 26-95 infection by soluble human Plxdc2-FcStrep on HaCaT cells. RRV-YFP 26-95 wt and RRV-YFP 26-95 gH-AELAAN were pre-incubated with hPlxdc2-FcStrep for 30min at room temperature. FcStrep alone was used as

328 control. YFP expression as indicator of infection was measured by flow cytometry. Infection in the
329 presence of 0.4nM FcStrep was set to 100% (MOI ~0.2, triplicates, error bars represent SD). **C)**
330 Inhibition of RRV 26-95 infection by soluble Plxdc2-Fc and EphB3-Fc on HaCaT cells. RRV-YFP 26-95 wt
331 and RRV-YFP 26-95 gH-AELAAN were pre-incubated with 100nM hPlxdc2-FcStrep, 10nM EphB3-Fc or
332 a combination of 100nM hPlxdc2-FcStrep and 10nM EphB3-Fc for 30min at room temperature.
333 FcStrep alone was used as control. YFP expression as indicator of infection was measured by flow
334 cytometry. Infection with FcStrep was set to 100% (MOI ~0.2, triplicates, error bars represent SD). **D)**
335 Inhibition of RRV 26-95 infection by soluble human Plxdc2-FcStrep on SLK cells and rhesus fibroblasts.
336 RRV-YFP 26-95 wt and RRV-YFP 26-95 gH-AELAAN were pre-incubated with 250nM hPlxdc2-FcStrep
337 for 30min at room temperature. FcStrep alone was used as control. YFP expression as indicator of
338 infection was measured by flow cytometry. Infection with FcStrep was set to 100% (MOI ~0.05-0.1,
339 triplicates, error bars represent SD). **E)** Raji cells were transduced with TwinStrep-tagged human
340 Plxdc1 and Plxdc2 (hPlxdc1-Strep/ hPlxdc2-Strep) expression constructs or an empty vector control,
341 briefly selected and infected with RRV-YFP 26-95 wt or RRV-YFP 26-95 gH-AELAAN normalized to
342 genome copies as determined by qPCR. Micrographs show representative infection of the indicated
343 cell pools. **F)** Lysates of transduced Raji cell pools were analyzed for Plxdc1/2-Strep expression by
344 Western blot. **G)** Quantification of (E) by flow cytometric analyses of YFP reporter gene expression as
345 indicator of infection.

346

347

348

349

350

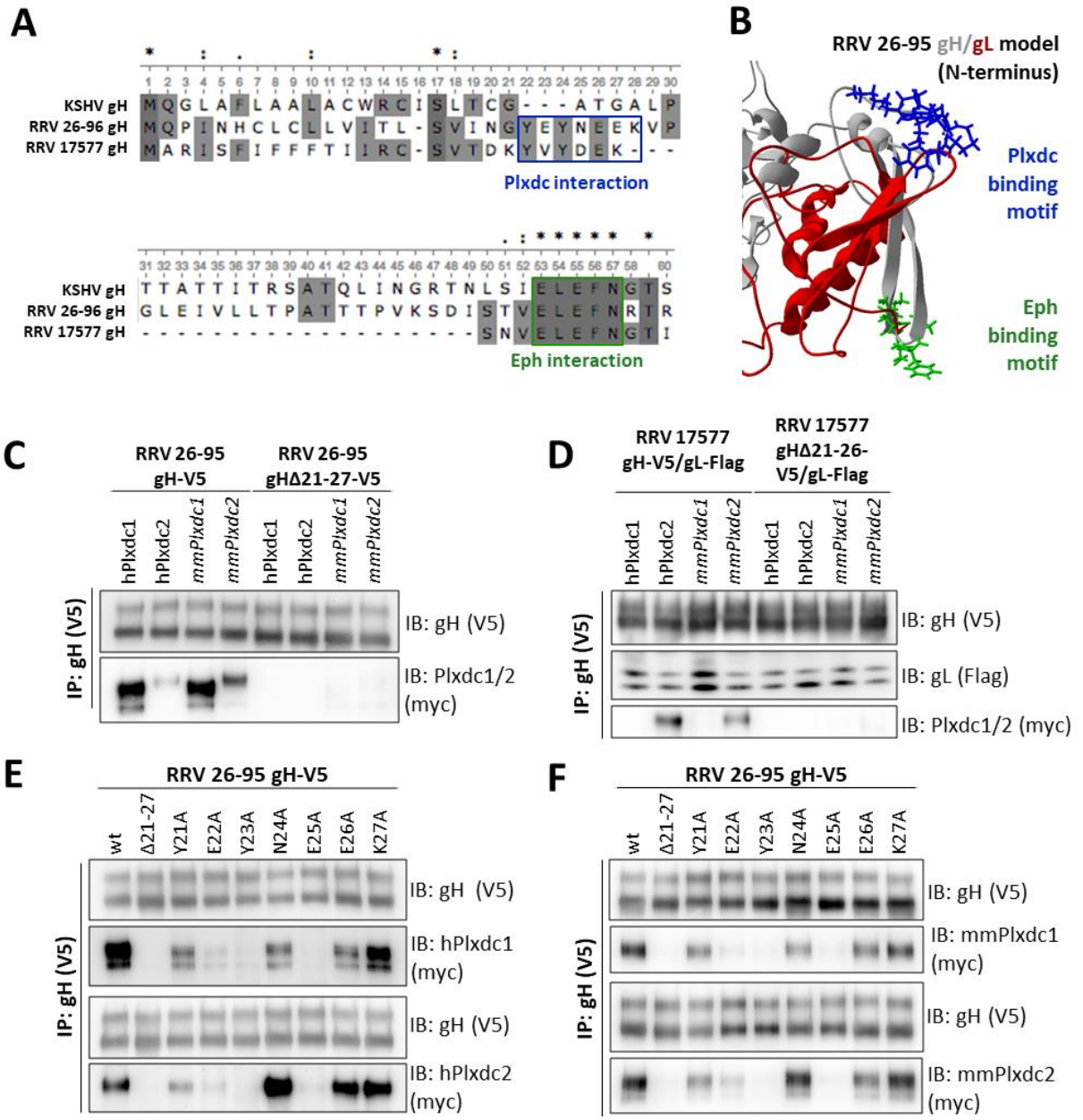

Figure 3 An amino acid sequence motif in the N-terminal region of RRV 26-95 and RRV 17577 gH is essential for the Plxdc-interaction. A) Multiple sequence alignment of the N-terminal region of gH of KSHV and the two RRV isolates 26-95 and 17577. Boxes indicate the binding motives for Eph receptors (green) and Plxdc receptors (blue). **B)** Homology-based structure prediction of the RRV 26-95 gH/gL complex based on the crystal structure of the EBV gH/gL complex (PDB number 3PHF) using the Iterative Threading ASSembly Refinement (I-TASSER) server and the CO-THreader (COTH) algorithms for protein-protein complex structure and multi-chain protein threading. The Eph receptor interaction motif is shown in green, the Plxdc interaction motif is shown in blue, gL is shown in red, gH is shown in grey. **C)** Deletion of the Plxdc-interaction motif in RRV 26-95 gH (amino acid 21-27, "YEYNEEK") abrogates gH interaction with Plxdc1 and Plxdc2. V5-tagged gH wt or gHΔ21-27 were immunoprecipitated in the presence of full-length human or macaca mulatta Plxdc1-myc or Plxdc2-myc using monoclonal antibody to the V5-tag. Precipitates were analyzed by Western blot. **D)** Deletion of the Plxdc-interaction motif in RRV 17577 gH (amino acid 21-26, "YVYDEK") abrogates gH interaction with Plxdc2. V5-tagged gH wt or gHΔ21-26 was co-expressed with Flag-tagged RRV 17577 gL. gH-V5/gL-Flag complexes were immunoprecipitated in the presence of full-length human or macaca mulatta Plxdc1-myc or Plxdc2-myc using monoclonal antibody to the V5-tag. Precipitates were analyzed by Western blot. **E)** Mutational scan of Plxdc-interaction motif (amino acid 21-27,

369 “YEYNEEK”) of RRV 26-95 gH identifies human Plxdc1/2-interacting residues. V5-tagged gH mutants
370 were immunoprecipitated in the presence of full-length human Plxdc1-myc or Plxdc2-myc using
371 monoclonal antibody to the V5-tag. Precipitates were analyzed by Western blot. RRV gHΔ21-27
372 serves as negative control. **F)** Mutational scan of Plxdc-interaction motif (amino acid 21-27,
373 “YEYNEEK”) of RRV 26-95 gH identifies rhesus macaque Plxdc1/2-interacting residues. V5-tagged gH
374 mutants were immunoprecipitated in the presence of full-length human Plxdc1-myc or Plxdc2-myc
375 using monoclonal antibody to the V5-tag. Precipitates were analyzed by Western blot. RRV gHΔ21-27
376 serves as negative control. Abbreviations: IP: immunoprecipitation, IB: immunoblotting, h: human,
377 mm: macaca mulatta (rhesus macaque).

378

379

380

A

Name	Mutation	Eph binding	Plxdc1/2 binding
RRV 26-95	wt	+	+
RRV 26-95 gH-AELAAN	gH V51A-E54A-E55A	-	+
RRV 26-95 gHΔ21-27	gH aa21-27 deletion	+	-
RRV 26-95 gHΔ21-27-AELAAN	gH aa21-27 deletion, V51A-E54A- E55A	-	-

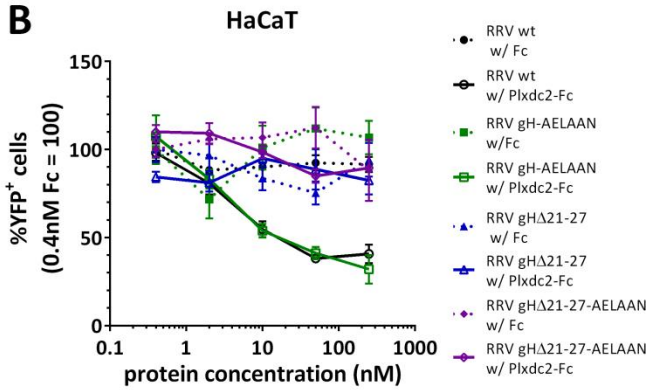

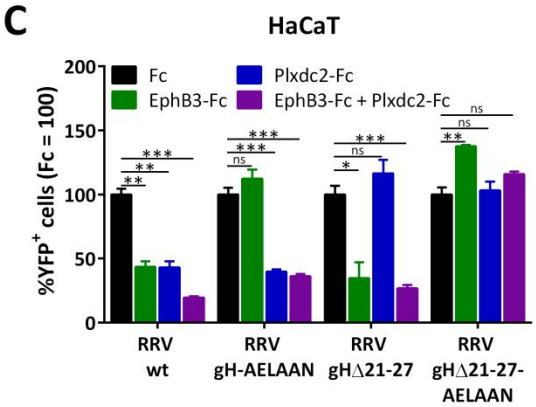

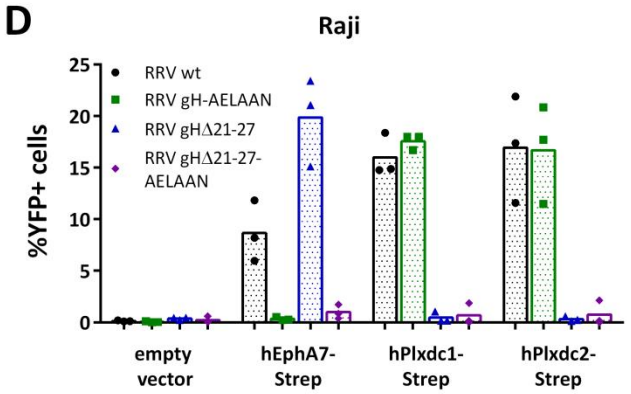

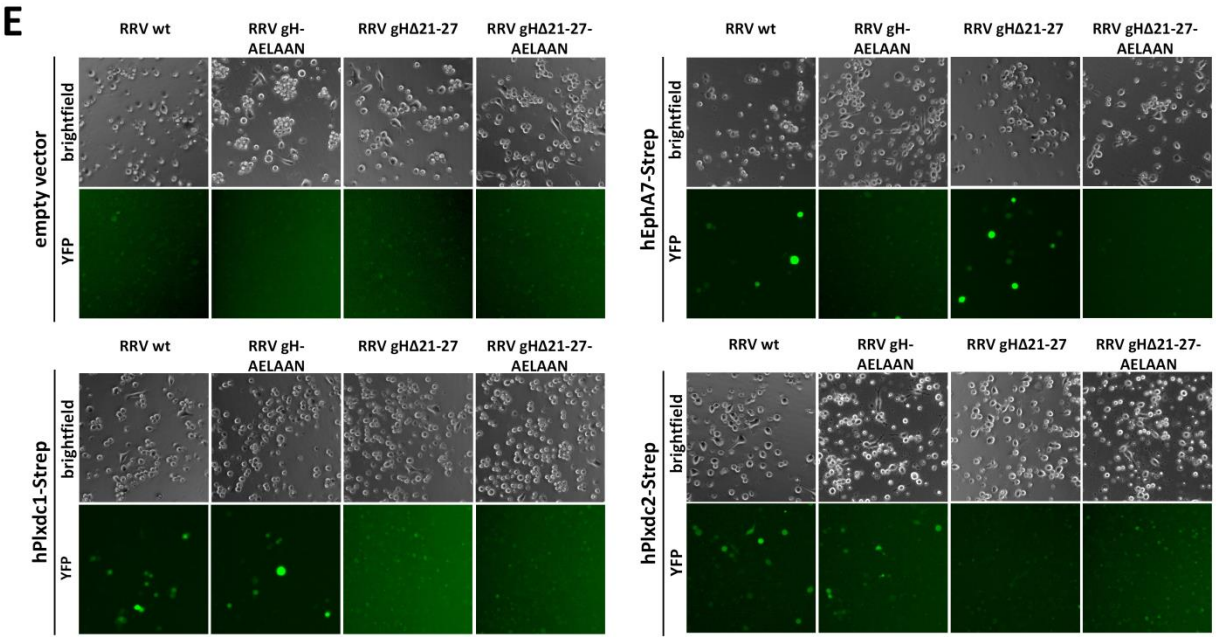

Figure 4 Deletion of the seven amino acid Plxdc-binding motif is sufficient to detarget RRV 26-95 from Plxdc receptors A) List of BAC-derived recombinant viruses and introduced mutations used in this figure. **B)** Dose-dependent inhibition of RRV-YFP 26-95 infection by soluble human Plxdc2-FcStrep on HaCaT cells. RRV-YFP 26-95 wt, RRV-YFP 26-95 gH-AELAAN, RRV-YFP 26-95 gHΔ21-27 and RRV-YFP 26-95 gHΔ21-27-AELAAN were pre-incubated with hPlxdc2-FcStrep for 30min at room temperature. FcStrep alone was used as control. YFP expression as indicator of infection was measured by flow cytometry. Infection in the presence of 0.4nM FcStrep was set to 100% (MOI ~0.05, triplicates, error bars represent SD). **C)** Inhibition of RRV 26-95 infection by soluble Plxdc2-Fc and EphB3-Fc on HaCaT cells. RRV-YFP 26-95 wt, RRV-YFP 26-95 gH-AELAAN, RRV-YFP 26-95 gHΔ21-27 and RRV-YFP 26-95 gHΔ21-27-AELAAN were pre-incubated with 100nM hPlxdc2-FcStrep, 10nM

392 EphB3-Fc or a combination of 100nM hPlxdc2-FcStrep and 10nM EphB3-Fc for 30min at room
393 temperature. FcStrep alone was used as control. YFP expression as indicator of infection was
394 measured by flow cytometry. Infection with FcStrep was set to 100% (MOI ~0.1-0.2, triplicates, error
395 bars represent SD). **D)** Raji cells were transduced with TwinStrep-tagged human EphA7, Plxdc1 or
396 Plxdc2 (hEphA7-Strep, hPlxdc1-Strep, hPlxdc2-Strep) expression constructs or an empty vector
397 control, briefly selected and infected with RRV-YFP 26-95 wt, RRV-YFP 26-95 gH-AELAAN, RRV-YFP
398 26-95 gHΔ21-27 or RRV-YFP 26-95 gHΔ21-27-AELAAN normalized to genome copies as determined by
399 qPCR. YFP expression as indicator of infection was measured by flow cytometry. The mean across
400 three independent sets of RRV stocks is indicated by columns. The means of individual triplicate
401 infections for each set of RRV stocks are given as symbols within the respective columns. **E)**
402 Micrographs show representative infection of one set of RRV stocks in (D).

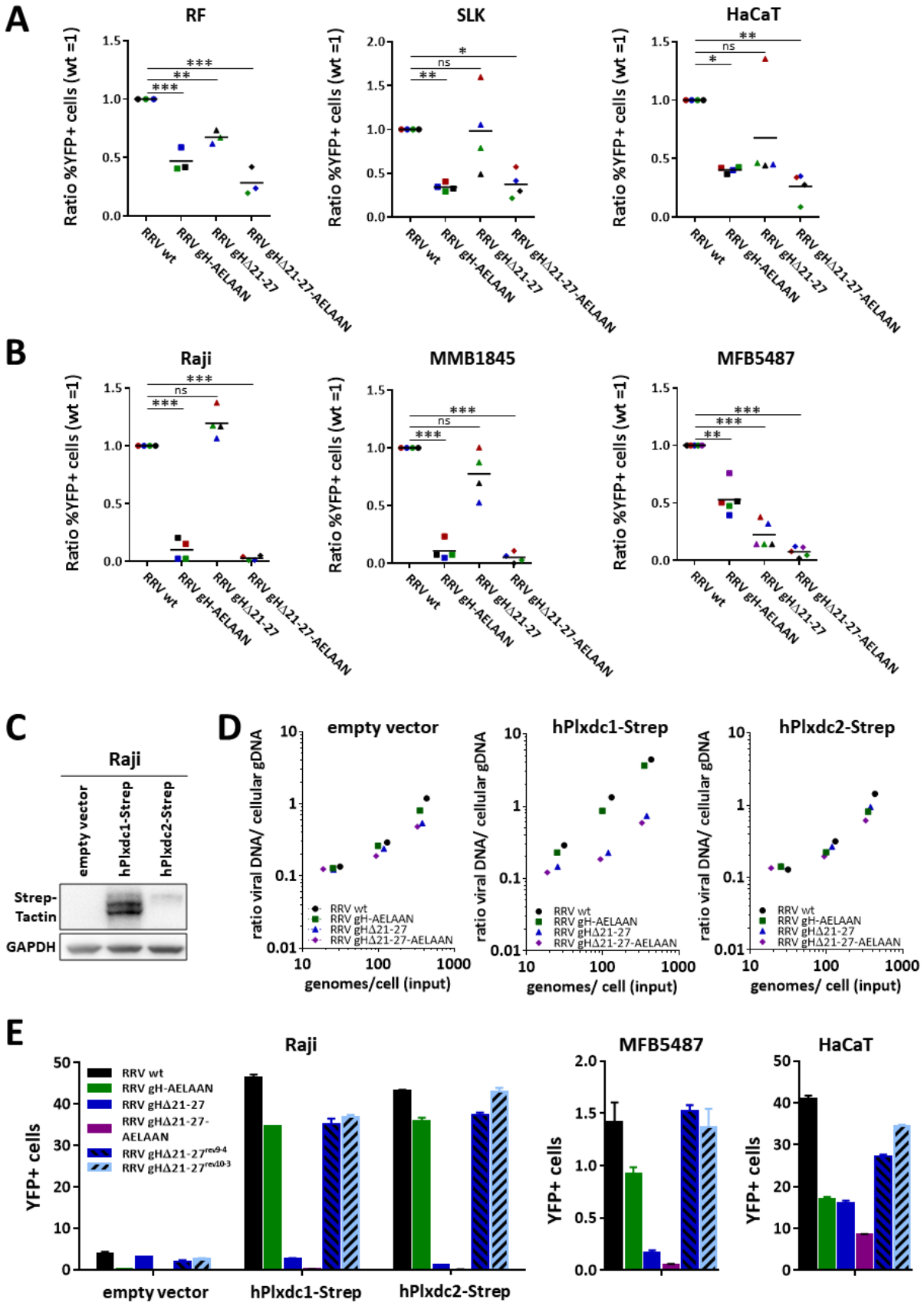

Figure 5 The contribution of the RRV 26-95 gH-Plxdc interaction to infection is cell type-specific and may in part be dependent on attachment effects. A) RRV 26-95 deleted in the Plxdc-interaction motif exhibits reduced specific infectivity on HaCaT and RF, but not SLK cells. Target cells were infected with RRV-YFP 26-95 wt, RRV-YFP 26-95 gH-AELAAN, RRV-YFP 26-95 gHΔ21-27 or RRV-YFP

408 26-95 gHΔ21-27-AELAAN normalized to genome copies as determined by qPCR. YFP expression as
409 indicator of infection was measured by flow cytometry and normalized to RRV-YFP 26-95 wt
410 infection. Means of individual normalized infections with three (RF) or four (HaCaT, SLK) independent
411 sets of RRV stocks are given as symbols of different color. Sets with RRV-YFP 26-95 wt infection in an
412 MOI range of 0.05 - 1 were used for analysis. The mean across the independent sets of RRV stocks is
413 indicated by black lines. **B)** RRV 26-95 deleted in the Plxdc-interaction motif exhibits reduced specific
414 infectivity on MFB5487, but not Raji and MMB1845 cells. Target cells were infected with RRV-YFP 26-
415 95 wt, RRV-YFP 26-95 gH-AELAAN, RRV-YFP 26-95 gHΔ21-27 or RRV-YFP 26-95 gHΔ21-27-AELAAN
416 normalized to genome copies as determined by qPCR. YFP expression as indicator of infection was
417 measured by flow cytometry and normalized to RRV-YFP 26-95 wt infection. Means of individual
418 normalized infections with four (Raji, MMB1845) or five (MFB5487) independent sets of RRV stocks
419 are given as symbols of different color. Sets with RRV-YFP 26-95 wt infection exceeding 1% were used
420 for analysis. The mean across the independent sets of RRV stocks is indicated by black lines. **C)**
421 Western blot analysis of Raji cells transduced with TwinStrep-tagged human Plxdc1 and Plxdc2
422 (hPlxdc1-Strep/ hPlxdc2-Strep) expression constructs or an empty vector control. **D)** Attachment of
423 RRV 26-95 on transduced Raji cells is affected by hPlxdc1-Strep, but not hPlxdc2-Strep
424 overexpression. Cells, analyzed in (C), were incubated with cold virus at the indicated concentrations
425 at 4°C for 30min followed by genomic DNA isolation. The ratio of viral to cellular DNA as
426 measurement for attached virus was calculated based on ΔCt values of a genomic (CCR5) and a viral
427 locus (ORF73/ LANA) as determined by qPCR and plotted against input viral genome number. **E)** Re-
428 introduction of the seven amino acid motif crucial for Plxdc-interaction rescues RRV-YFP 26-95
429 gHΔ21-27 infection. Transduced Raji cells, analyzed in (C), were infected with RRV-YFP 26-95 wt, RRV-
430 YFP 26-95 gH-AELAAN, RRV-YFP 26-95 gHΔ21-27, RRV-YFP 26-95 gHΔ21-27-AELAAN or two RRV-YFP
431 26-95 gHΔ21-27 revertants (RRV-YFP 26-95 gHΔ21-27^{rev9-4}, RRV-YFP 26-95 gHΔ21-27$^{rev10-3}$) normalized
432 to genome copies as determined by qPCR. YFP expression as indicator of infection was measured by
433 flow cytometry (triplicates, error bars represent SD).

434 **MATERIAL AND METHODS**

435 **Cells.** Human embryonic kidney (HEK) 293T cells (RRID:CVCL_0063) (laboratory of Tobias Moser), SLK cells
436 (RRID:CVCL_9569) (NIH AIDS Research and Reference Reagent program), rhesus monkey fibroblasts (RF)
437 (laboratory of Prof. Rüdiger Behr) and HaCaT human keratinocytes (RRID:CVCL_0038) were cultured in
438 Dulbecco's Modified Eagle Medium (DMEM), high glucose, GlutaMAX, 25mM HEPES (Thermo Fisher Scientific)
439 supplemented with 10% fetal calf serum (FCS) (Thermo Fisher Scientific), and 50µg/ml gentamycin (PAN
440 Biotech). iSLK cells (laboratory of Don Ganem, Novartis Institutes for BioMedical Research, Emeryville, CA, USA)
441 were maintained in DMEM supplemented with 10% FCS, 50µg/ml gentamycin, 2.5µg/ml puromycin (InvivoGen)
442 and 250µg/ml G418 (Carl Roth). Raji cells (RRID:CVCL_0511) (laboratory of Jens Gruber), MFB5487 (a clonal cell
443 line established from macaca fascicularis PBMC, immortalized by infection with herpesvirus papio; a kind gift
444 from Ulrike Sauermann) and MMB1845 cells (a clonal cell line established from macaca mulatta PBMC,
445 immortalized by infection with herpesvirus papio; a kind gift from Ulrike Sauermann) were cultured in RPMI
446 (Thermo Fisher Scientific) supplemented with 10% FCS and 50µg/ml gentamycin.

447 **BAC mutagenesis and virus production.** RRV recombinants (RRV gHΔ21-27, RRV gHΔ21-27-AELAAN) were
448 generated based on BAC35-8 (43) and RRV gH-AELAAN (21) respectively, using a two-step, markerless λ-red-
449 mediated BAC recombination strategy as described by Tischer et al. (33). In short, recombination cassettes
450 were generated from the pEPKanS template by polymerase chain reaction (PCR) with Phusion High Fidelity DNA
451 polymerase (Thermo Fisher Scientific) using long oligonucleotides (Ultramers; purchased from Integrated DNA
452 Technologies (IDT)) (see S1 Table for a complete list of primers). Recombination cassettes were transformed
453 into RRV-YFP-carrying GS1783 followed by kanamycin selection, and subsequent second recombination under
454 1% L(+)arabinose (Sigma-Aldrich)-induced I-SceI expression. Colonies were verified by PCR of the mutated
455 region followed by sequence analysis (Macrogen), pulsed-field gel electrophoresis and restriction fragment
456 length polymorphism. For this purpose, bacmid DNA was isolated by standard alkaline lysis from 5ml liquid
457 cultures. Subsequently, the integrity of bacmid DNA was analyzed by digestion with restriction enzyme *Xho*I
458 and separation in 1% PFGE agarose (Bio-Rad) gels and 0.5×TBE buffer by pulsed-field gel electrophoresis at 6
459 V/cm, 120-degree field angle, switch time linearly ramped from 1s to 5s over 16 h (CHEF DR III, Bio-Rad).
460 Infectious RRV-YFP recombinants were generated as described previously (21). In short, bacmid DNA
461 (NucleoBond Xtra Midi) was transfected into 293T cells using GenJet Ver. II (Signagen) according to
462 manufacturer's instructions. Transfected 293T cells were transferred onto a confluent rhesus monkey
463 fibroblasts monolayer two days after transfection and co-cultivated until a visible cytopathic effect (CPE) was
464 observed. For virus stocks preparations, confluent primary rhesus monkey fibroblasts were inoculated with
465 infectious supernatant of 293T/rhesus monkey fibroblast co-cultures. After multiple rounds of replication virus-
466 containing RF supernatant was clarified by centrifugation (4750g, 10 minutes), concentrated by overnight
467 centrifugation (4200rpm, 4°C) and careful aspiration of approximately 95% of the supernatant. The pellet was
468 resuspended overnight in the remaining liquid. Stocks of wt and recombinant viruses were aliquoted and
469 stored at -80°C. Mutations were verified by PCR amplification of the respective region followed by sequence
470 analysis (Macrogen).

471 **Plasmids.** The pcDNA4 vector containing full-length EphB3 (ref|BC052968|, pcDNA-EphB3-myc), pcDNA6aV5
472 vectors containing RRV/KSHV gH and gL coding sequences (ref|GQ994935.1|, pcDNA6aV5-KSHV-gH, pcDNA3.1-
473 KSHV-gL-Flag (13); ref|AF210726.1|, pcDNA6aV5-RRV-26-95-gH, pcDNA3.1-RRV-26-95-gL-Flag (14, 44);
474 ref|AF083501.3|, pcDNA6aV5-RRV-17577-gH, pcDNA3.1-RRV-17577-gL-Flag (14)) were described elsewhere.
475 RRV 26-95/ RRV 17577 recombinant gH constructs were generated based on pcDNA6aV5-RRV-26-95-gH or
476 pcDNA6aV5-RRV-17577-gH, respectively, using 'Round the Horn Site-directed mutagenesis. Expression
477 plasmids pcDNA4-hPlxdc1-myc (Homo sapiens, full-length, ref |NM_020405.5|) and pcDNA4-hPlxdc2-myc
478 (Homo sapiens, full-length, ref |NM_032812.9|) were generated by PCR based restriction cloning. The soluble
479 ectodomain of human Plxdc2 (amino acids 31-453) without signal peptide was inserted behind a heterologous
480 signal peptide of murine IgG-kappa into pAB61Strep by PCR based restriction cloning, resulting in a C-terminally
481 fused IgG1 Fc-fusion protein with a C-terminal tandem Strep-Tag (pPlxdc2-FcStrep) as described previously
482 (45). Expression plasmids pcDNA4-mmPlxdc1-myc (macaca mulatta, full-length, ref |XM_028836436.1|) and
483 pcDNAmmPlxdc2-myc (macaca mulatta, full-length, ref |XM_028826043.1|) were generated based on PCR-
484 amplified gBlock gene fragments (purchased from IDT) of the regions varying from human Plxdc1 (nt1-1200)
485 and Plxdc2 (nt1-1401), respectively, and ligated in the respective PCR-amplified backbone (pcDNA4hPlxdc1-
486 myc, pcDNA4hPlxdc2-myc) by exonuclease-based Gibson-assembly (Gibson Assembly Mastermix, New England
487 Biolabs). pLenti CMV Blast DEST (706-1) (a gift from Eric Campeau & Paul Kaufman (Addgene plasmid #17451))
488 constructs carrying a human Plxdc1-TwinStrep or Plxdc2-TwinStrep expression cassette (pLenti-CMV-Blast-
489 Plxdc1-Strep/ pLenti-CMV-Blast-Plxdc2-Strep) were based on pcDNA4-hPlxdc1-myc/ pcDNA4-hPlxdc2-myc,
490 which were PCR-amplified and ligated using exonuclease-based Gibson-assembly. pLenti-CMV-Blast-EphA7-
491 Strep was described before (19). (See S1 Table for a complete list of primers and constructs).
492

493 **Recombinant proteins.** Recombinant, soluble FcStrep and Plxdc2-FcStrep-fusion proteins were purified under
494 native conditions by Strep-Tactin chromatography from 293T cell culture supernatant. 293T cells were
495 transfected using Polyethylenimine "Max" (PEI) (Polysciences) (46) as described before (19) with pAB61Strep
496 or pPlxdc2-FcS. The protein-containing cell culture supernatant was filtered through 0.22µm PES membranes
497 (Millipore) and passed over 0.5ml of a Strep-Tactin Superflow (IBA Lifesciences) matrix in a gravity flow
498 Omniprep column (BioRad). Bound protein was washed with approximately 50ml phosphate buffered saline pH
499 7.4 (PBS) and eluted in 1ml fractions with 3mM desthiobiotin (Sigma-Aldrich) in PBS. Protein-containing
500 fractions were pooled and buffer exchange to PBS via VivaSpin columns (Sartorius) was performed. Protein
501 concentration was determined by absorbance at 280nm. Aliquots were frozen and stored at −80°C.
502 Recombinant, human, soluble EphB3-Fc (5667-B3-050) was purchased from R&D Systems.

503 **Lentivirus production and transduction**. For production of lentiviral particles, 10cm cell culture grade petri
504 dishes of approximately 80% confluent 293T cells were transfected with 1.4µg pMD2.G (VSV-G envelope
505 expressing plasmid, a gift from Didier Trono (Addgene plasmid #12259), 3.6µg psPAX2 (Gag-Pol expression
506 construct, a gift from Didier Trono (Addgene plasmid #12260), and 5µg of lentiviral expression constructs
507 (pLenti CMV Blast DEST (706-1), pLenti-CMV-Blast-EphA7-Strep, pLenti-CMV-Blast-Plxdc1-Strep, pLenti-CMV-
508 Blast-Plxdc2-Strep) using PEI as described before (19). The supernatant containing the pseudotyped lentiviral

509 particles was harvested 2 to 3 days after transfection and filtered through 0.45µm CA membranes (Millipore).
510 For transduction, lentivirus stocks were used at a 1:5 dilution unless stated otherwise. After 48h, the selection
511 antibiotic blasticidin (Invivogen) was added to a final concentration of 10µg/ml. After initial selection the
512 blasticidin concentration was reduced to 5µg/ml.

513 **Quantitative realtime-PCR-based viral genome copy number analysis and virus attachment assay.**
514 Concentrated virus samples were treated with DNAseI (0.1 units/µl) to remove any non-encapsidated DNA
515 (37°C, overnight). Subsequently, DNAseI was deactivated and viral capsids were disrupted by heating the
516 samples to 95°C for 30 minutes. Realtime-PCR (qPCR) was performed on a StepOne Plus cycler (Thermo Fisher
517 Scientific) in 20µl reactions using the SensiFAST Probe Hi-ROX Kit (Bioline) (cycling conditions: 3min initial
518 denaturation at 95°C, 40 cycles 95°C for 10s and 60°C for 35s). All primer-probe sets were purchased from IDT
519 as complete PrimeTime qPCR Assays (primer:probe ratio = 4:1). Samples were analyzed in technical triplicates.
520 A series of five 10-fold dilutions of bacmid DNA was used as standard for absolute quantification of viral
521 genome copies based on qPCR of ORF73 for RRV (see S1 Table for a complete list of primers). For virus
522 attachment assays transduced Raji cells were incubated with ice-cold virus dilutions at the indicated
523 concentrations, normalized to genomes per cell, at 4°C for 30min. After three washes with ice-cold PBS
524 genomic DNA was isolated using the ISOLATE II Genomic DNA Kit (Bioline) according to manufacturer's
525 instructions. Genome copies of used input virus preparations were determined after overnight DNAseI digest
526 as described above. Relative values of bound viral genomes to cellular DNA were calculated on the basis of ΔCt
527 values for viral genomic loci (ORF73 for RRV) and a cellular genomic locus (CCR5) using the same conditions
528 described above. For attachment assays all samples were analyzed in technical duplicates.

529 **Infection assays, blocking experiments and flow cytometry.** For infection assays cells were plated at 50 000
530 cells/cm^2 (SLK, HaCaT, Raji), 25 000 cells/cm^2 (RF) or 200 000 cells/ml (Raji, MFB5487, MMB1845) respectively.
531 One day after plating (for adherent cells lines) or directly after plating (for suspension cell lines), cells were
532 infected with the indicated amounts of virus. Adherent cells lines were harvested 24h post infection by brief
533 trypsinization, followed by addition of 5% FCS in PBS to inhibit trypsin activity. Suspension cell lines were
534 harvested 48h post infection (24h post infection for transduced Raji cells) by pipetting. Subsequently, cells
535 were pelleted by centrifugation (1200rpm, 10min), washed once with PBS, re-pelleted and fixed in PBS
536 supplemented with 4% formaldehyde (Carl Roth). Block of RRV infection with soluble decoy receptor was
537 assayed by infection with virus inocula that were pre-incubated with the indicated concentrations of soluble
538 EphB3-Fc, hPlxdc1-Fc, hPlxdc2-Fc or Fc alone at room temperature for 30min. Calculation of molarity was based
539 on diametric proteins. Cell harvest and preparation for flow cytometry analyses was performed as described
540 above. A minimum of 5 000 – 10 000 cells was analyzed per sample for YFP expression on a LSRII flow
541 cytometer (BD Biosciences). Data was analyzed using Flowing Software (Version 2.5).

542 **Immunoprecipitation and Western blot analysis.** For interaction analysis of gH-V5/gL-Flag complexes with
543 Plxdc1/2, 293T cells were transfected using PEI as described before. Lysates of 293T cells transfected with the
544 respective expression constructs for recombination gH-V5/gL-Flag complexes were prepared in NP40 lysis
545 buffer (1% Nonidet P40 Substitute (Sigma-Aldrich), 150mM NaCl (Sigma-Aldrich), 50mM HEPES (VWR), 1mM

546 EDTA (Amresco) with freshly added Protease Inhibitor Cocktail, General Use (Amresco)) and protein content
547 was determined by Bradford assay using Roti-Quant (Roth) according to manufacturer's instructions. 20µg total
548 protein was denatured in 1x SDS sample buffer (Morris formulation) at 95°C for 5min, separated by
549 polyacrylamide gel electrophoresis (PAGE) using 8–16% Tris-Glycine polyacrylamide gradient gels (Thermo
550 Fisher Scientific) with Tris-Glycine SDS running buffer (25mM Tris, 192mM glycine, 0.1% SDS) and transferred to
551 0.45µm (0.22µm for blots containing gL) Polyvinylidendifluorid (PVDF) membranes (200mA/Gel, max 30V, 1h in
552 Towbin buffer (25mM Tris, 192mM glycine) with 20% methanol) in a wet tank system (Mini Blot Module,
553 Thermo Fisher). The membranes were blocked in 5% dry milk powder in TBS-T (5mM Tris, 15mM NaCl, 0.05%
554 Tween20) for 1h, at room temperature, washed once in TBS-T and incubated with the respective antibodies for
555 2h at room temperature or overnight at 4°C (see S1 Table for a complete list of antibodies). After three washes
556 with TBS-T, the membranes were incubated with the respective HRP-conjugated secondary antibody in 5% dry
557 milk powder in TBS-T for 1h at room temperature washed three times in TBS-T and imaged on an ECL
558 ChemoCam 3.2 Imager (Intas) using Immobilon Forte Western HRP substrate (Merck Millipore). For pulldown of
559 gH-V5 or gH-V5/ gL-Flag complexes, the amount of input lysate between wt and mutant gH constructs was
560 normalized to gH expression as determined by Western blot and diluted to equal volume with cell lysate from
561 non-transfected 293T cells prior to immunoprecipitation. Subsequently, lysates were incubated with 0.5µg V5-
562 tag antibody (Bio-Rad) and ProteinG sepharose (GenScript) overnight at 4°C with agitation. After three washes
563 in NP40 lysis buffer, ProteinG beads with pre-coupled complexes were incubated overnight at 4°C with
564 agitation with lysate of full-length human or macaca mulatta Plxdc1-myc or Plxdc2-myc expression plasmid
565 transfected 293T cells normalized to Plxdc expression. Volumes were adjusted with lysate from untransfected
566 293T cells. ProteinG beads were collected by brief centrifugation and washed 3 times in NP40 lysis buffer.
567 Precipitates were heated in 2x SDS sample buffer (95°C, 5min) and analyzed by Western blot as described
568 above. For co-immunoprecipitation of soluble Plxdc1/2-Strep constructs with gH-V5/gL-Flag and EphB3-myc,
569 supernatant of Plxdc1/2-FcStrep transfected 293T cells was incubated with StrepTactinXT beads (IBA) overnight
570 at 4°C with agitation. After three washes in NP40 lysis buffer, StrepTactinXT beads with pre-coupled Plxdc1/2-
571 Strep were incubated overnight at 4°C with agitation with equal amounts of lysate of full-length human EphB3-
572 myc, RRV 26-95 gH-V5/gL-Flag or 17577 gH-V5/gL-Flag expression plasmid transfected 293T cells or the
573 indicated combinations. Volumes were adjusted with lysate of untransfected 293T cells.

574 **Structure prediction and analysis.** Homology based structure prediction was performed using the Iterative
575 Threading ASSembly Refinement (I-TASSER) server on standard settings for structure prediction of RRV 26-95
576 gH and gL based on the crystal structure of the EBV gH/gL complex (3PHF). Modeling of the RRV 26-95 gH/gL
577 complex was additionally performed using both the SPRING and CO-THreader algorithms for protein-protein
578 complex structure and multi-chain protein threading with no differences between determined structures.
579 Resulting I-TASSER structures were aligned to the gH/gL CO-THreader model with the VMD 1.9.3 OpenGL RMSD
580 Trajectory Tool based on amino acids 25 to 62 of gH (RMSD of 0.344Å) and amino acids 2 to 100 of gL (RMSD of
581 2.697Å) to generate the depicted model. All further analyses and visualizations were performed using VMD
582 1.9.3 OpenGL.

583 **Mathematical and statistical analysis**. Statistical difference between groups was determined by unpaired
584 Student's t-tests followed by Bonferroni correction for multiple comparisons. All Statistical analyses were
585 performed with GraphPad Prism version 6. For all statistics, *: p-value < 0.05, **: p-value < 0.01, ***: p-value <
586 0.001, ns: not significant.

587 **ACKNOWLEDGMENTS**

588 This work was supported by grants to A.S.H. from the Deutsche Forschungsgemeinschaft (HA 6013/1,
589 HA 6013/4-1) and the Interdisciplinary Center for Clinical Research Erlangen (IZKF, grant J44), by the
590 German Research foundation, grants CRC 796, TP B1 to A.E., by grant RO1 AI072004 from the
591 National Institutes of Health (NIH) to R.C.D., and by base grant RR00168 from the NIH to the New
592 England Primate Research Center.

593 **LITERATURE**

594 1. Desrosiers RC, Sasseville VG, Czajak SC, Zhang X, Mansfield KG, Kaur A, Johnson RP, Lackner AA,
595 Jung JU. 1997. A herpesvirus of rhesus monkeys related to the human Kaposi's sarcoma-
596 associated herpesvirus. J Virol 71:9764–9769.

597 2. Searles RP, Bergquam EP, Axthelm MK, Wong SW. 1999. Sequence and genomic analysis of a
598 Rhesus macaque rhadinovirus with similarity to Kaposi's sarcoma-associated
599 herpesvirus/human herpesvirus 8. J Virol 73:3040–3053.

600 3. O'Connor CM, Kedes DH. 2007. Rhesus Monkey Rhadinovirus: A Model for the Study of KSHV,
601 p. 43–69. *In* Boshoff, C, Weiss, RA (eds.), Kaposi Sarcoma Herpesvirus: New Perspectives.
602 Springer Berlin Heidelberg.

603 4. Shin YC, Jones LR, Manrique J, Lauer W, Carville A, Mansfield KG, Desrosiers RC. 2010.
604 Glycoprotein gene sequence variation in rhesus monkey rhadinovirus. Virology 400:175–186.

605 5. Bilello JP, Morgan JS, Damania B, Lang SM, Desrosiers RC. 2006. A Genetic System for Rhesus
606 Monkey Rhadinovirus: Use of Recombinant Virus To Quantitate Antibody-Mediated
607 Neutralization. J Virol 80:1549–1562.

608 6. Estep RD, Powers MF, Yen BK, Li H, Wong SW. 2007. Construction of an Infectious Rhesus
609 Rhadinovirus Bacterial Artificial Chromosome for the Analysis of Kaposi's Sarcoma-Associated
610 Herpesvirus-Related Disease Development. J Virol 81:2957–2969.

611 7. Bilello JP, Lang SM, Wang F, Aster JC, Desrosiers RC. 2006. Infection and Persistence of Rhesus
612 Monkey Rhadinovirus in Immortalized B-Cell Lines. J Virol 80:3644–3649.

613 8. Wong SW, Bergquam EP, Swanson RM, Lee FW, Shiigi SM, Avery NA, Fanton JW, Axthelm MK.
614 1999. Induction of B cell hyperplasia in simian immunodeficiency virus-infected rhesus
615 macaques with the simian homologue of Kaposi's sarcoma-associated herpesvirus. J Exp Med
616 190:827–840.

617 9. Orzechowska BU, Powers MF, Sprague J, Li H, Yen B, Searles RP, Axthelm MK, Wong SW. 2008.
618 Rhesus macaque rhadinovirus-associated non-Hodgkin lymphoma: animal model for KSHV-
619 associated malignancies. Blood 112:4227–4234.

620 10. Bruce AG, Bielefeldt-Ohmann H, Barcy S, Bakke AM, Lewis P, Tsai C-C, Murnane RD, Rose TM.
621 2012. Macaque Homologs of EBV and KSHV Show Uniquely Different Associations with Simian
622 AIDS-related Lymphomas. PLoS Pathog 8:e1002962.

623 11. Marshall VA, Labo N, Hao X-P, Holdridge B, Thompson M, Miley W, Brands C, Coalter V, Kiser R,
624 Anver M, Golubeva Y, Warner A, Jaffe ES, Piatak M, Wong SW, Ohlen C, MacAllister R, Smedley
625 J, Deleage C, Del Prete GQ, Lifson JD, Estes JD, Whitby D. 2018. Gammaherpesvirus infection
626 and malignant disease in rhesus macaques experimentally infected with SIV or SHIV. PLOS
627 Pathog 14:e1007130.

628 12. Umbach JL, Strelow LI, Wong SW, Cullen BR. 2010. Analysis of rhesus rhadinovirus microRNAs
629 expressed in virus-induced tumors from infected rhesus macaques. Virology 405:592–599.

630 13. Hahn AS, Kaufmann JK, Wies E, Naschberger E, Panteleev-Ivlev J, Schmidt K, Holzer A, Schmidt
631 M, Chen J, König S, Ensser A, Myoung J, Brockmeyer NH, Stürzl M, Fleckenstein B, Neipel F.
632 2012. The ephrin receptor tyrosine kinase A2 is a cellular receptor for Kaposi's sarcoma–
633 associated herpesvirus. Nat Med 18:961–966.

634 14. Hahn AS, Desrosiers RC. 2013. Rhesus Monkey Rhadinovirus Uses Eph Family Receptors for
635 Entry into B Cells and Endothelial Cells but Not Fibroblasts. PLoS Pathog 9:e1003360.

636 15. TerBush AA, Hafkamp F, Lee HJ, Coscoy L. 2018. A Kaposi's Sarcoma-Associated Herpesvirus
637 Infection Mechanism Is Independent of Integrins α3β1, αVβ3, and αVβ5. J Virol 92:e00803-18,
638 /jvi/92/17/e00803-18.atom.

639 16. Chen J, Zhang X, Schaller S, Jardetzky TS, Longnecker R. 2019. Ephrin Receptor A4 is a New
640 Kaposi's Sarcoma-Associated Herpesvirus Virus Entry Receptor. mBio 10:e02892-18,
641 /mbio/10/1/mBio.02892-18.atom.

642 17. Hahn AS, Desrosiers RC. 2014. Binding of the Kaposi's sarcoma-associated herpesvirus to the
643 ephrin binding surface of the EphA2 receptor and its inhibition by a small molecule. J Virol
644 88:8724–8734.

645 18. Kumar B, Chandran B. 2016. KSHV Entry and Trafficking in Target Cells-Hijacking of Cell Signal
646 Pathways, Actin and Membrane Dynamics. Viruses 8.

647 19. Großkopf AK, Schlagowski S, Hörnich BF, Fricke T, Desrosiers RC, Hahn AS. 2019. EphA7
648 Functions as Receptor on BJAB Cells for Cell-to-Cell Transmission of the Kaposi's Sarcoma-
649 Associated Herpesvirus and for Cell-Free Infection by the Related Rhesus Monkey Rhadinovirus.
650 J Virol 93:e00064-19, /jvi/93/15/JVI.00064-19.atom.

651 20. Möhl BS, Chen J, Longnecker R. 2019. Gammaherpesvirus entry and fusion: A tale how two
652 human pathogenic viruses enter their host cells, p. 313–343. *In* Advances in Virus Research.
653 Elsevier.

654 21. Großkopf AK, Ensser A, Neipel F, Jungnickl D, Schlagowski S, Desrosiers RC, Hahn AS. 2018. A
655 conserved Eph family receptor-binding motif on the gH/gL complex of Kaposi's sarcoma-
656 associated herpesvirus and rhesus monkey rhadinovirus. PLOS Pathog 14:e1006912.

657 22. Hahn AS, Bischof GF, Großkopf AK, Shin YC, Domingues A, Gonzalez-Nieto L, Rakasz EG, Watkins
658 DI, Ensser A, Martins MA, Desrosiers RC. 2019. A Recombinant Rhesus Monkey Rhadinovirus
659 Deleted of Glycoprotein L Establishes Persistent Infection of Rhesus Macaques and Elicits
660 Conventional T Cell Responses. J Virol JVI.01093-19, jvi;JVI.01093-19v1.

661 23. Croix BSt. 2000. Genes Expressed in Human Tumor Endothelium. Science 289:1197–1202.

662 24. Carson-Walter EB, Watkins DN, Nanda A, Vogelstein B, Kinzler KW, St Croix B. 2001. Cell surface
663 tumor endothelial markers are conserved in mice and humans. Cancer Res 61:6649–6655.

664 25. Miller-Delaney SFC, Lieberam I, Murphy P, Mitchell KJ. 2011. Plxdc2 is a mitogen for neural
665 progenitors. PloS One 6:e14565.

666 26. Lee HK, Bae HR, Park HK, Seo IA, Lee EY, Suh DJ, Park HT. 2005. Cloning, characterization and
667 neuronal expression profiles of tumor endothelial marker 7 in the rat brain. Brain Res Mol Brain
668 Res 136:189–198.

669 27. Miller SFC, Summerhurst K, Rünker AE, Kerjan G, Friedel RH, Chédotal A, Murphy P, Mitchell KJ.
670 2007. Expression of Plxdc2/TEM7R in the developing nervous system of the mouse. Gene Expr
671 Patterns GEP 7:635–644.

672 28. Nanda A, Buckhaults P, Seaman S, Agrawal N, Boutin P, Shankara S, Nacht M, Teicher B, Stampfl
673 J, Singh S, Vogelstein B, Kinzler KW, St. Croix B. 2004. Identification of a Binding Partner for the
674 Endothelial Cell Surface Proteins TEM7 and TEM7R. Cancer Res 64:8507–8511.

675 29. Cheng G, Zhong M, Kawaguchi R, Kassai M, Al-Ubaidi M, Deng J, Ter-Stepanian M, Sun H. 2014.
676 Identification of PLXDC1 and PLXDC2 as the transmembrane receptors for the multifunctional
677 factor PEDF. eLife 3:e05401.

678 30. Lee HK, Seo IA, Park HK, Park HT. 2006. Identification of the basement membrane protein
679 nidogen as a candidate ligand for tumor endothelial marker 7 in vitro and in vivo. FEBS Lett
680 580:2253–2257.

681 31. Uhlen M, Fagerberg L, Hallstrom BM, Lindskog C, Oksvold P, Mardinoglu A, Sivertsson A, Kampf
682 C, Sjostedt E, Asplund A, Olsson I, Edlund K, Lundberg E, Navani S, Szigyarto CA-K, Odeberg J,
683 Djureinovic D, Takanen JO, Hober S, Alm T, Edqvist P-H, Berling H, Tegel H, Mulder J, Rockberg J,
684 Nilsson P, Schwenk JM, Hamsten M, von Feilitzen K, Forsberg M, Persson L, Johansson F,
685 Zwahlen M, von Heijne G, Nielsen J, Ponten F. 2015. Tissue-based map of the human proteome.
686 Science 347:1260419–1260419.

687 32. Matsuura H, Kirschner AN, Longnecker R, Jardetzky TS. 2010. Crystal structure of the Epstein-
688 Barr virus (EBV) glycoprotein H/glycoprotein L (gH/gL) complex. Proc Natl Acad Sci 107:22641–
689 22646.

690 33. Tischer BK, Smith GA, Osterrieder N. 2010. En Passant Mutagenesis: A Two Step Markerless Red
691 Recombination System, p. 421–430. *In* Braman, J (ed.), In Vitro Mutagenesis Protocols. Humana
692 Press, Totowa, NJ.

693 34. Li Q, Turk SM, Hutt-Fletcher LM. 1995. The Epstein-Barr virus (EBV) BZLF2 gene product
694 associates with the gH and gL homologs of EBV and carries an epitope critical to infection of B
695 cells but not of epithelial cells. J Virol 69:3987–3994.

696 35. Nguyen C, Kamil J. 2018. Pathogen at the Gates: Human Cytomegalovirus Entry and Cell
697 Tropism. Viruses 10:704.

698 36. Hirai H, Maru Y, Hagiwara K, Nishida J, Takaku F. 1987. A novel putative tyrosine kinase
699 receptor encoded by the eph gene. Science 238:1717–1720.

700 37. Pasquale EB. 2010. Eph receptors and ephrins in cancer: bidirectional signalling and beyond.
701 Nat Rev Cancer 10:165–180.

702 38. Zhang Z-Z, Hua R, Zhang J-F, Zhao W-Y, Zhao E-H, Tu L, Wang C-J, Cao H, Zhang Z-G. 2015. TEM7
703 (PLXDC1), a key prognostic predictor for resectable gastric cancer, promotes cancer cell
704 migration and invasion. Am J Cancer Res 5:772–781.

705 39. Carpenter RL, Paw I, Zhu H, Sirkisoon S, Xing F, Watabe K, Debinski W, Lo H-W. 2015. The gain-
706 of-function GLI1 transcription factor TGLI1 enhances expression of VEGF-C and TEM7 to
707 promote glioblastoma angiogenesis. Oncotarget 6:22653–22665.

708 40. Czekierdowski A, Stachowicz N, Czekierdowska S, Łoziński T, Gurynowicz G, Kluz T. 2018.
709 Prognostic significance of TEM7 and nestin expression in women with advanced high grade
710 serous ovarian cancer. Ginekol Pol 89:135–141.

711 41. Kim GH, Won JE, Byeon Y, Kim MG, Wi TI, Lee JM, Park Y-Y, Lee J-W, Kang TH, Jung ID, Shin BC,
712 Ahn HJ, Lee YJ, Sood AK, Han HD, Park Y-M. 2018. Selective delivery of PLXDC1 small interfering
713 RNA to endothelial cells for anti-angiogenesis tumor therapy using CD44-targeted chitosan
714 nanoparticles for epithelial ovarian cancer. Drug Deliv 25:1394–1402.

715 42. Falchetti ML, D'Alessandris QG, Pacioni S, Buccarelli M, Morgante L, Giannetti S, Lulli V, Martini
716 M, Larocca LM, Vakana E, Stancato L, Ricci-Vitiani L, Pallini R. 2019. Glioblastoma endothelium
717 drives bevacizumab-induced infiltrative growth via modulation of PLXDC1. Int J Cancer
718 144:1331–1344.

719 43. Hahn AS, Großkopf AK, Jungnickl D, Scholz B, Ensser A. 2016. Viral FGARAT Homolog ORF75 of
720 Rhesus Monkey Rhadinovirus Effects Proteasomal Degradation of the ND10 Components SP100
721 and PML. J Virol 90:8013–8028.

722 44. Shin YC, Desrosiers RC. 2011. Rhesus Monkey Rhadinovirus ORF57 Induces gH and gL
723 Glycoprotein Expression through Posttranscriptional Accumulation of Target mRNAs. J Virol
724 85:7810–7817.

725 45. Hahn A, Birkmann A, Wies E, Dorer D, Mahr K, Sturzl M, Titgemeyer F, Neipel F. 2009. Kaposi's
726 Sarcoma-Associated Herpesvirus gH/gL: Glycoprotein Export and Interaction with Cellular
727 Receptors. J Virol 83:396–407.

728 46. Longo PA, Kavran JM, Kim M-S, Leahy DJ. 2013. Transient Mammalian Cell Transfection with
729 Polyethylenimine (PEI), p. 227–240. *In* Methods in Enzymology. Elsevier.

730

731